Developmental timing of CCM2 loss influences cerebral cavernous malformations in mice

Gwénola Boulday,[1,2] Noemi Rudini,[3] Luigi Maddaluno,[3] Anne Blécon,[1,2] Minh Arnould,[1,2] Alain Gaudric,[4] Françoise Chapon,[5] Ralf H. Adams,[6] Elisabetta Dejana,[3,7] and Elisabeth Tournier-Lasserve[1,2,4]

[1]Institut National de la Santé et de la Recherche Médicale, UMR-S 740, 75010 Paris, France
[2]Université Paris 7-Denis Diderot, Faculté de Médecine, Site Lariboisière, Paris, F-75010, France
[3]Fondazione Italiana per la Ricerca sul Cancro Institute of Molecular Oncology (IFOM), 20139 Milano, Italy
[4]AP-HP, Groupe Hospitalier Saint-Louis Lariboisiere-Fernand-Widal, Paris, F-75010, France
[5]Department of Pathology, Centre Hospitalier Universitaire, Avenue Côte de Nacre, 14032 Caen, France
[6]Max Planck Institute for Molecular Biomedicine, Faculty of Medicine, Department of Tissue Morphogenesis and University of Münster, 48149 Münster, Germany
[7]Department of Biomolecular Sciences and Biotechnologies, Milan University School of Sciences, 20133 Milan, Italy

Cerebral cavernous malformations (CCM) are vascular malformations of the central nervous system (CNS) that lead to cerebral hemorrhages. Familial CCM occurs as an autosomal dominant condition caused by loss-of-function mutations in one of the three *CCM* genes. Constitutive or tissue-specific ablation of any of the *Ccm* genes in mice previously established the crucial role of *Ccm* gene expression in endothelial cells for proper angiogenesis. However, embryonic lethality precluded the development of relevant CCM mouse models. Here, we show that endothelial-specific *Ccm2* deletion at postnatal day 1 (P1) in mice results in vascular lesions mimicking human CCM lesions. Consistent with *CCM1/3* involvement in the same human disease, deletion of *Ccm1/3* at P1 in mice results in similar CCM lesions. The lesions are located in the cerebellum and the retina, two organs undergoing intense postnatal angiogenesis. Despite a pan-endothelial *Ccm2* deletion, CCM lesions are restricted to the venous bed. Notably, the consequences of *Ccm2* loss depend on the developmental timing of Ccm2 ablation. This work provides a highly penetrant and relevant CCM mouse model.

CORRESPONDENCE
Elisabeth Tournier-Lasserve:
tournier-lasserve@
univ-paris-diderot.fr

Abbreviations used: AJ, adherens junction; CCM, cerebral cavernous malformation; CNS, central nervous system; E, embryonic day; EC, endothelial cell; iCCM, inducible CCM KO mice; LEF, lymphoid enhancer factor; P, postnatal day; PCP, planar cell polarity; TCF, T cell factor; TJ, tight junction; Wnt, Wingless and Int.

Cerebral cavernous malformations (CCMs) lesions consist of densely packed vascular sinusoids lined by a thin endothelium with rare subendothelial cells and no intervening parenchyma (Russel and Rubinstein, 1989; Clatterbuck et al., 2001). Ultrastructural analysis of CCM lesions showed defective tight junctions (TJ) between endothelial cells (ECs). The lesions form predominantly in the central nervous system (CNS), but ~5% of the patients also show lesions in the retina (Labauge et al., 2007; Riant et al., 2010).

The prevalence has been estimated to be up to 0.5% in the general population. CCM occurs as a sporadic (80% of patients) or a familial disease (20% of patients), after an autosomal dominant pattern of inheritance. Sporadic patients most often have a single CCM lesion, whereas patients affected by a hereditary form of the disease have multiple lesions and show a progressive increase in lesion number over time. Symptoms include headaches, seizures, and focal neurological deficits caused by cerebral hemorrhages. The major risk for patients is the recurrence of hemorrhages. Neurosurgery is the only therapy offered today; however, it is not always possible depending on the lesion location within the CNS.

Familial CCM disease is caused by heterozygous germline mutations in any of the three *CCM* genes identified so far (*CCM1/KRIT1*,

N. Rudini and L. Maddaluno contributed equally to this paper.

The Rockefeller University Press $30.00
J. Exp. Med. Vol. 208 No. 9 1835-1847
www.jem.org/cgi/doi/10.1084/jem.20110571

CCM2/MGC4607, and *CCM3/PDCD10*; Craig et al., 1998; Laberge-le Couteulx et al., 1999; Liquori et al., 2003; Denier et al., 2004; Bergametti et al., 2005). Recently, a "two-hit" mechanism has been demonstrated in human ECs within the CCM lesions (Gault et al., 2005; Akers et al., 2009; Pagenstecher et al., 2009).

The three *CCM* genes encode scaffold proteins without any sequence homology. In the recent past, in vitro data obtained in different cell types identified numerous CCM protein partners that form complexes involved in various intracellular signaling pathways (Faurobert and Albiges-Rizo, 2010). Consistent with their involvement in CCM pathogenesis, the three CCM proteins can interact in a cytosolic ternary complex, where CCM2 acts as a bridge between CCM1 and CCM3 (Hilder et al., 2007). However, the in vivo functions of this ternary complex remain unclear.

When associated with the integrin β1-binding protein ICAP-1, KRIT1 shuttles from the cytosol to the nucleus; its function there remains to be determined. CCM2 interaction with KRIT1 modulates KRIT1 trafficking by sequestering KRIT1 in the cytoplasm (Zawistowski et al., 2005). KRIT1 is a Rap1 effector and stabilizes the endothelial cell–cell junctions (Glading et al., 2007). Recently, physical interaction between KRIT1 and CCM2 was proven to be required for CCM protein localization at endothelial cell–cell junctions (Stockton et al., 2010). KRIT1 has also been involved in vascular lumenization and polarization of the endothelial tube in vitro (Lampugnani et al., 2010).

Several studies have provided new insights into CCM protein functions in vitro, including cytoskeletal remodeling, cell–cell junction homeostasis, lumen formation, and polarization. However, it remains to be clarified which protein complexes and signaling pathways are relevant in vivo, and how the loss of function of any of the three CCM proteins might explain the etiology of the CCM disease. To this aim, relevant mouse models for the CCM disease are needed to understand the molecular mechanisms involved in lesion pathogenesis. Moreover, relevant mouse models reproducing CCM lesions would allow development of preclinical therapeutic studies (Leblanc et al., 2009; Yadla et al., 2010).

Over the past few years, several groups reported constitutive or tissue-specific KO mice for all three *CCM* genes. Homozygous *Ccm1*-deficient mice die at midgestation with defects in the vascular structure and impaired arterial morphogenesis (Whitehead et al., 2004). We and others have shown that endothelial-specific ablation of *Ccm2* severely affects embryonic angiogenesis, leading to lethality at midgestation (Boulday et al., 2009; Whitehead et al., 2009). In contrast, neuronal-specific and smooth muscle cell–specific deletion of *Ccm2* does not affect the vascular development (Whitehead et al., 2009). In a recent publication, He et al. (2010) reported similar results using constitutive or tissue-specific deletion of *Ccm3* in mice. Together, those studies demonstrated that endothelial expression of the CCM proteins is crucial for proper angiogenesis. However, the embryonic lethality of these previous mouse models limited their use to analyze the role of the CCM proteins during cerebral angiogenesis and CCM pathophysiology.

In this study, to bypass embryonic lethality, we deleted the *Ccm2* gene in the mouse in an inducible, EC-specific manner. Postnatal day 1 (P1) deletion of *Ccm2* resulted in vascular lesions that are strikingly similar to human CCM lesions in the cerebellum and retina. Using the same strategy, P1 deletion of *Ccm1* or *Ccm3* led to similar cerebellar and retinal lesions. We showed that CCM2 lesion development is restricted to the venous bed. We also demonstrated the existence of a time window for the effects of *Ccm2* deletion, related to a developmental stage with intense angiogenesis. Here, we describe a relevant mouse model for CCM disease with complete penetrance and fast development of the disease allowing us to follow the lesion development.

RESULTS

Endothelial-specific *Ccm2* deletion at P1 results in vascular malformations mimicking human CCM lesions in the CNS

To bypass the embryonic lethality previously encountered in the Tie2Cre;*Ccm2* KO mouse model (Boulday et al., 2009), we crossed *Ccm2* floxed mice with the endothelial-specific, tamoxifen-inducible *Cdh5(PAC)*-CreERT2 mice (Wang et al., 2010). *Rosa*26-Stop^{fl}-LacZ reporter mice were used to monitor the tamoxifen-induced Cre/Lox recombination (Soriano, 1999). As assessed by XGal staining, high recombination efficiency was obtained after tamoxifen treatment (Fig. S1, A–F). Unless otherwise mentioned, the genotype of *Ccm2*-ablated mice (iCCM2 for inducible CCM2 KO) was *Cdh5(PAC)*-CreERT2; *Ccm2* $^{fl/Del}$; *Rosa*-Stop^{fl}-LacZ (see Materials and methods for details of mouse breeding).

Animals were tamoxifen injected at P1 and were analyzed at different time points, from P6 through 3 wk of age (Table I). The estimated survival median for iCCM2 animals calculated by the Kaplan-Meier test is 17 d (with a $P < 0.001$ of significance for survival compared with controls; Fig. 1 A). At P8, all iCCM2 animals were alive and grossly undistinguishable from controls. They did not show any significant difference in weight (4.14 ± 0.6 g for iCCM2 versus 4.51 ± 0.7 g for controls). However, from P6 onward, we were able to distinguish the iCCM2 animals upon dissection of the brain (for ∼80% of the P6-P7 iCCM2 and 100% from P8 onward) and a clear aggravation of the vascular phenotype over time was observed (Fig. S2 A). P1 deletion of *Ccm2* resulted in the development of CCM lesions within the CNS

Table I. Number of iCCM2 analyzed after P1 deletion

Age of analysis	Total numbers of iCCM2	iCCM2 with cerebral CCM lesions[a]/ total number of iCCM2
P6-7	12	10/12
P8-10	30	30/30
P11-15	10	10/10
P16-19	4	4/4

[a]Visible lesions upon dissection.

of all iCCM2 animals. Interestingly, the lesions were exclusively located in the cerebellum (Fig. 1 B). Histology showed cerebellar lesions composed of dilated vessels full of blood cells (Fig. 1 B, bottom). In more severe cases, lesions form multiple caverns, sometimes with evident signs of hemorrhage (Fig. 1 B, right). The mouse CCM lesions phenocopy lesions found in human CCM patients (Fig. 1 D, left). At P8, lesions of different severity were found in the same iCCM2 animal, from small vessel dilations to large caverns (Fig. S2, B–F). From P9 onward, some iCCM2 animals were found dead in their cage. When possible, analysis of these animals before death revealed extensive cerebral hemorrhages, located mostly around the multiple caverns composing CCM lesions but also scattered all over the brain (Fig. 1 B, right; and not depicted). In addition to CCM lesions, *Ccm2* deletion at P1 in the mouse induced dilation of vessels from the pial surface of the cerebellum (Fig. 1 B, middle).

Because 5% of familial CCM patients show vascular lesions in the retina, we analyzed the retinal vessels in iCCM2 mice. All iCCM2 animals showed CCM vascular malformations located at the periphery of the retinal vascular plexus in both eyes (Fig. 1 C). Again, the vascular lesions obtained after *Ccm2* deletion in the mouse retina mimic the CCM retinal lesions found in patients (Fig. 1 D, right).

We used the same gene targeting strategy to invalidate endothelial *Ccm1* or *Ccm3* in mice. Tamoxifen-induced deletion of *Ccm1* or *Ccm3* at P1 resulted in CCM malformations in the CNS of all iCCM1 and iCCM3 animals analyzed ($n = 4$ in each group). The CCM1 and CCM3 lesions were comparable to the lesions obtained after *Ccm2* deletion in terms of location (within the cerebellum and at the periphery of the retina) and phenotype (Fig. S3).

We established a relevant mouse model for the human CCM with a complete penetrance and a fast development of CCM lesions from single to multiple hemorrhagic caverns (Fig. 1 B and Fig. S2, C–F). Moreover, P1 deletion of any of the three *Ccm* genes resulted in a similar phenotype according to what is established for the human CCM disease.

Endothelial cell–cell junctions are altered in CCM2 KO cells in vitro and in CCM2 lesions

To investigate whether part of the phenotype could be related to altered endothelial cell–cell junctions, we analyzed the expression and organization of junctional proteins in ECs in vitro and in vivo in cerebellar vessels of iCCM2 mice.

We abrogated CCM2 expression by treating ECs derived from *Ccm2*$^{fl/fl}$ mice with TAT-Cre recombinase (Fig. S4 A).

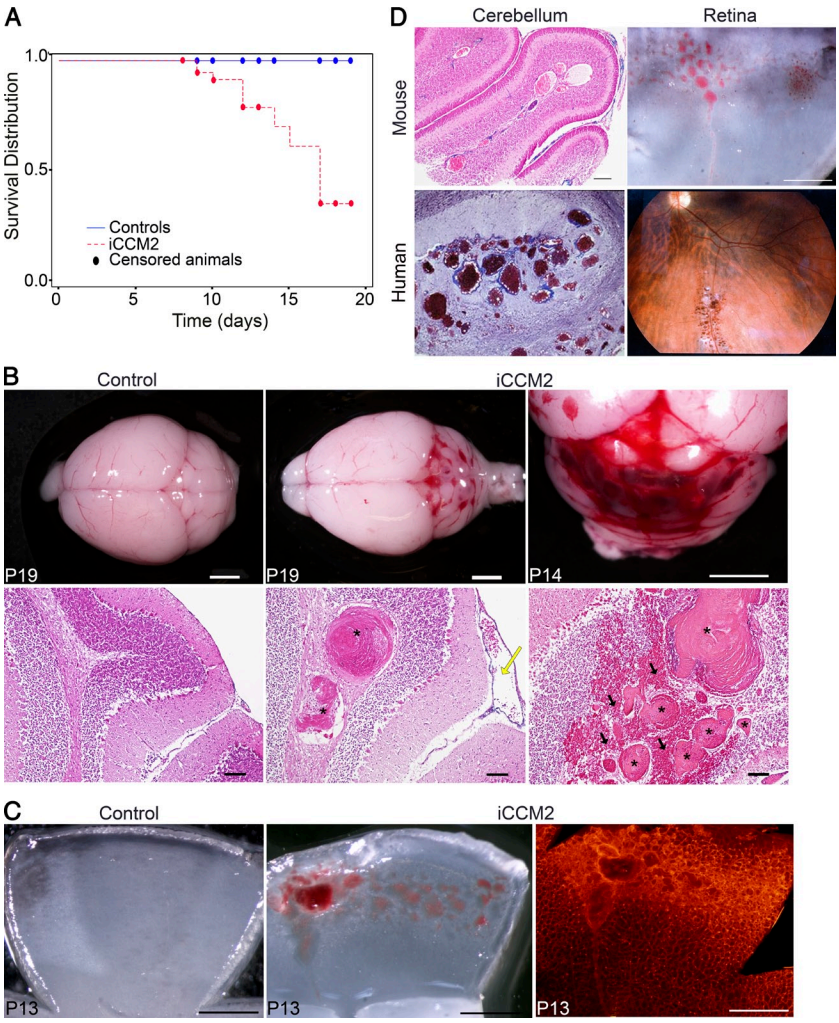

Figure 1. Endothelial *Ccm2* deletion at P1 results in CCM malformations mimicking the human CCM lesions in the cerebellum and in the retina. All animals were injected at P1 with 10 µl tamoxifen (equivalent to 20 µg) and dissected at the indicated time. Genotypes of inducible CCM2 KO (iCCM2) and control animals were respectively *Cdh5(PAC)*-CreERT2; *Ccm2*$^{Del/fl}$ and *Cdh5(PAC)*-CreERT2; *Ccm2*$^{+/fl}$. (A) Kaplan-Meier survival curve from the control group (blue line, $n = 110$) and the iCCM2 group (dotted red line, $n = 56$). Circles represent censored animals, which were sacrificed for analysis. (B) Control and iCCM2 mouse brains upon dissection (top) and after H&E staining (bottom; $n = 6$ in each group from 4 different litters, analyzed between P11 and P19). CCM malformations, located in the cerebellum of iCCM2 animals, are composed by single or multiple caverns (asterisks) with extensive hemorrhage (black arrows) around the juxtaposed vascular cavities. Note the dilation of meningeal vessels in the iCCM2 (yellow arrow). (C) Control and iCCM2 mouse retinas at P13 upon dissection (left and middle) and after isolectin-B4 staining (right, $n = 7$ in each group from 4 different litters, analyzed between P11 and P15). (D) Mouse lesions phenocopy human CCM lesions. (left) Histology of the cerebral lesions in mouse and human. (right) Mouse retina upon dissection and human retinal angiography Bars: 2 mm (B, top); 500 µm (C and D, mouse retina); 100 µm (B [bottom] and D [mouse cerebellum]).

In the absence of CCM2, ECs lost correct organization of both TJ and adherens junctions (AJ; Fig. S4, B–D). Expression of the TJ component claudin-5 was essentially absent in CCM2 KO ECs and was undetectable at junctions. ZO.1 also presented a discontinuous and weak staining at cell–cell contacts, whereas JAM-A and Afadin appeared diffuse on the cell membrane (Fig. S4 D). AJ components such as VE-cadherin, β-catenin, and α-catenin were significantly reduced by CCM2 deletion and presented a dotted, faint, and irregular staining at junctions (Fig. S4 D and not depicted). Conversely, plakoglobin, another member of the catenin family, was strongly increased, whereas PECAM1 was unchanged (Fig. S4 C). Thus, in CCM2-null ECs, the overall composition and organization of junctions is strongly altered. In addition, endothelial monolayer permeability in the absence of CCM2 was significantly increased (Fig. S4 E).

We then analyzed endothelial junction organization in vivo in iCCM2 brain vasculature (Fig. 2). Staining of junctional components supported data obtained in cultured ECs. Indeed, claudin-5 or ZO.1 were correctly expressed in peri-lesion vessels, but strongly reduced in abnormally dilated and hemorrhagic CCM lesions (Fig. 2 B). In addition, the AJ protein VE-cadherin appeared to be disorganized and was not clearly concentrated at intercellular endothelial cell–cell contacts within the lesion, as compared with normal cerebral vessels in iCCM2 animals (Fig. 2 C).

Overall, these data indicate that CCM2 is required for proper cell–cell junction architecture in ECs in vitro and that CCM2 deletion in vivo results in impaired EC junction architecture in CCM2 lesions.

To investigate the mechanism of the strong reduction in claudin-5 expression upon CCM2 ablation, we evaluated the major regulators of claudin-5 expression, including the Akt–FoxO1 signaling pathway (Brunet et al., 1999; Burgering and Kops, 2002; Zhang et al., 2002; Daly et al., 2004; Taddei et al., 2008), the transcription factor Sex-determining region Y-box-18 (SOX18), and the ETS ternary complex ELK3 (Fontijn et al., 2008). Phosphorylation of Akt was enhanced in confluent CCM2 KO ECs compared with control ECs, accompanied by a strong phosphorylation of FoxO1 (Fig. S5 A). These data excluded Akt–FoxO1 pathway involvement in claudin-5 reduction in CCM2-null ECs. In contrast, SOX18 expression was found to be reduced by 50% by quantitative RT-PCR in CCM2 KO versus control ECs, whereas ELK3 expression was not modified (Fig. S5 B). This result supports the idea that alteration in SOX18 expression

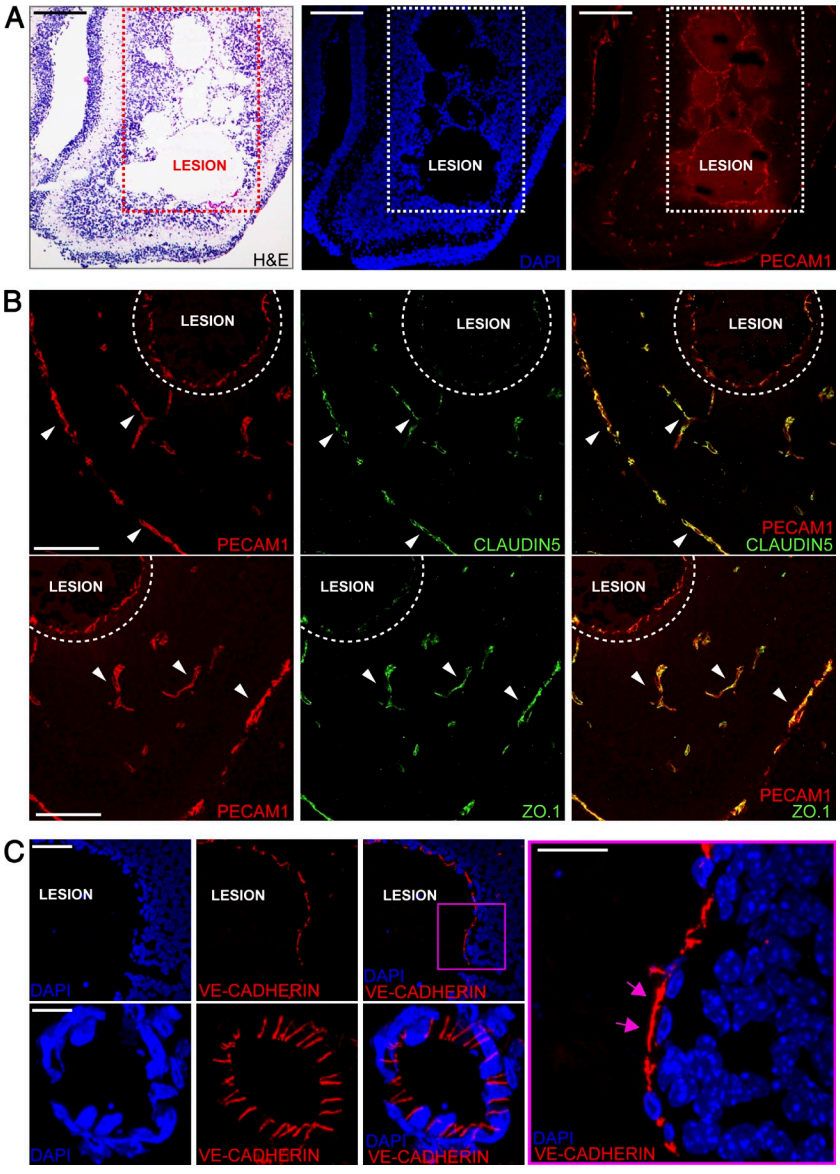

Figure 2. *Ccm2* deletion alters AJ and TJ organization in CCM lesions. Analysis of cell–cell junctions in CCM2 malformations on frozen sections of iCCM2 brain. For all immunofluorescence experiments, cell nuclei are visualized with DAPI (blue). Data are representative of 3 independent observations ($n = 5$ in each group, from 2 different litters). (A) H&E staining (left) and confocal microscopy analysis showing vessels stained using anti-PECAM1 (red, right). (B) Co-staining of the vessels using PECAM1 staining (red) and the TJ components (green) using claudin-5 (top) and ZO.1 (bottom). Claudin-5 and ZO.1 are normally expressed in peri-lesion vessels (arrowheads), whereas they are strongly down-regulated in abnormally dilated and hemorrhagic vessels of the lesion (dotted area). (C) VE-cadherin staining (red) of the endothelium lining lesion and peri-lesion vessels. (right) Magnification of the boxed area. Pink arrows indicate VE-cadherin expressed outside of the junctions. Bars: 200 µm (A); 100 µm (B); 60 µm (C, top); 4 µm (C, bottom and right).

could be one of the mechanisms responsible for the down-regulation of claudin-5 in the absence of CCM2.

The Wnt–β-catenin pathway is not involved in CCM2 lesion development in vivo

β-Catenin participates in the formation and stabilization of cadherin-based adhesion by forming a connection to the actin cytoskeleton (Dejana, 2010). β-Catenin is also a key element of the canonical Wnt (wingless and Int-1) signaling that promotes the nuclear localization of β-catenin by blocking the β-catenin destruction complex. Binding of β-catenin to cadherins can antagonize Wnt signaling by sequestering β-catenin at the membrane. Alteration of AJ promotes β-catenin nuclear translocation and the subsequent activation of T cell factor (TCF)/lymphoid enhancer factor (LEF) transcriptional complexes. KRIT1 is localized at the endothelial cell–cell junction and can be co-precipitated with β-catenin (Glading et al., 2007). Depletion of endothelial KRIT1 in vitro has been described to induce β-catenin delocalization from the membrane to the nucleus leading to increased β-catenin transcriptional activity (Glading and Ginsberg, 2010).

Interestingly, in CCM2 KO ECs in vitro, we also observed a delocalization of β-catenin from the membrane to the nucleus, suggesting β-catenin activation (unpublished data). However, TCF/LEF-β-catenin transcriptional activity, as detected using the TOPFlash reporter, which includes six TCF-binding sites, was not significantly modified in CCM2-null cells compared with controls (Fig. 3 A), suggesting that the Wnt–β-catenin pathway is not disregulated in CCM2-null ECs in vitro.

To investigate whether the Wnt–β-catenin signaling pathway is involved in vivo in the CCM pathogenesis, we assessed the β-catenin transcriptional activity in the absence of CCM2 in mice. Animals were crossed with the BAT-Gal reporter mouse (see Materials and methods for mating details), which drives β-galactosidase expression under the control of multimerized TCF/LEF binding sites for activated nuclear β-catenin. iCCM2; BAT-Gal mice were injected at P1 with tamoxifen to ablate *Ccm2*. Consistent with the previous study by Maretto et al. (2003), the β-catenin signaling was activated in the mouse cerebellum at P8 (Fig. 3, B–I). We found a similar activation of the β-catenin signaling in controls or iCCM2 cerebellum, mostly located in the Purkinje cell layer, and in some ECs within the white matter. In contrast, the endothelium lining the CCM malformations did not show any evidence of β-catenin signaling pathway activation at P8, neither in the cerebellum nor in the retina (Fig. 3, G–I; and not depicted), suggesting an absence of Wnt–β-catenin pathway involvement in iCCM2 lesions at the time of analysis.

CCM lesions specifically affect the venous bed and not the arterial compartment

Retinal vessels develop after birth in the mouse, after a very well defined and organized pattern (Dorrell and Friedlander, 2006; Fruttiger, 2007). Within the first week of life a vascular plexus develops at the inner surface of the retina, from the central retina toward the periphery. At this stage, the strict

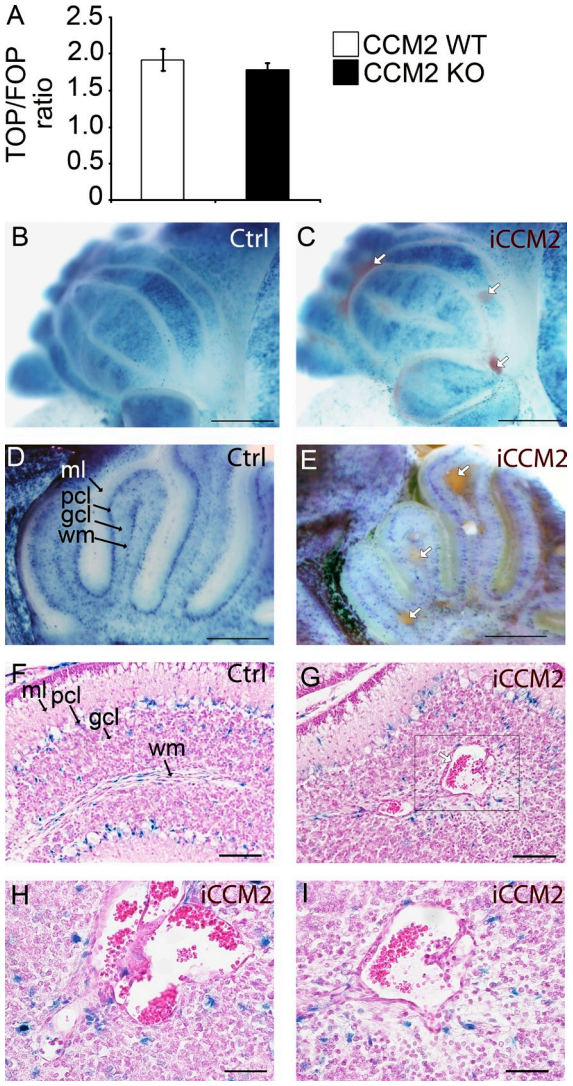

Figure 3. *Ccm2* deletion has no significant effect on Wnt–β-catenin signaling pathway in CCM2 KO ECs in vitro and in iCCM2 lesions. (A) TCF/LEF-β-catenin transcriptional activity in CCM2 WT and null ECs in vitro was determined by transfecting CCM2 WT and KO ECs with the TOP-TK-Luc or the FOP-TK-Luc reporter constructs (containing WT or mutant Tcf/Lef binding sites, respectively, and a basal TK promoter, upstream a luciferase gene). Columns are means ± SD of triplicates from a representative experiment out of three performed. (B-I) Animals were bred with the BAT-Gal reporter mouse to assess β-catenin activation (see Materials and methods for breeding details). All animals were injected with tamoxifen at P1. XGal staining, performed on control and iCCM2 cerebellum, is shown ($n = 8$ in each group, from 3 different litters). White arrows show the CCM lesions in iCCM2 animals (in C, E, and G). In F–I, H&E staining was performed on cerebellum sections, after XGal staining. The box in G is magnified in I. H shows a CCM lesion composed of multiple juxtaposed caverns. Gcl, granular cell layer; ml, molecular layer; pcl, Purkinje cell layer; wm, white matter. Bars: 1 mm (B and C); 500 µm (D and E); 100 µm (F and G); 50 µm (H and I).

alternation between arteries (thin and straight with avascular spaces surrounding arteries) and veins (larger and more sinuous) can easily be distinguished using an isolectin-B4 staining (Fig. 4 A). Analyzing retina from 1-wk-old P1-ablated iCCM2 animals, we observed that CCM malformations at the periphery of the iCCM2 retinas were clearly restricted to veins and the surrounding capillaries (Fig. 4 A).

In utero *Ccm2* deletion led to vascular anomalies in the cerebral hemispheres, affecting cerebral rhinal veins and the surrounding capillaries (Fig. 4 B). In contrast, middle cerebral arteries remained normal. To further confirm that the arterial compartment is not affected by CCM lesion, we compared vessels from mice mated with either the *Rosa*26-Stop^{fl}-LacZ reporter mouse (to visualize all the vessels), or with the artery-specific *EphrinB2*^{tlacZ} reporter mouse (Fig. 4, A [right] and C; see Materials and methods for breeding details). XGal stainings showed that endothelium of the retinal and cerebral CCM lesions did not express the arterial-specific EphrinB2 marker. In addition, P1 deletion also resulted in dilation of vessels running along the cerebellar folia at the meningeal surface corresponding to dorsal cerebellar veins (Fig. 1 B; Nonaka et al., 2002).

Collectively, our results showed that *Ccm2* deletion affects the venous bed and leads to capillary-venous malformations.

Natural history of CCM lesions

A great advantage of animal models is the possibility to explore the etiology of the vascular malformations at very early stages to determine herein the natural history of the CCM lesion over time. We followed lesion development in the retina with an isolectin-B4 staining (Fig. 5). As early as P7, the vascular plexus was thicker at the venous leading edge of the retina in iCCM2 animals. Quantification of the vascular coverage at the venous leading edge showed a 29% increase in iCCM2 retinas compared with controls (Fig. 5 B; 0.56 ± 0.01 in controls versus 0.76 ± 0.01 in iCCM2; P = 0.0004; n = 4). By P9, the main veins were dilated in iCCM2 animals with abnormal capillaries at the periphery of the vascular plexus. In 3-wk-old control mice, the retinal vasculature was fully established, with 3 distinct plexuses. In contrast, at the periphery of iCCM2 retinas, it was not possible to distinguish different vascular plexuses. The vasculature from the lesion was composed by bubblelike vascular structures packed together. A 2,000-kD intracardiac FITC-Dextran injection confirmed that those abnormal vascular structures were lumenized (unpublished data).

To investigate the mechanisms of the increase in diameter of iCCM2 retinal vessels at P7, we assessed whether EC proliferation was altered in the absence of CCM2. Using a phospho-histone-3 staining, we could not detect any significant increase in EC proliferation in iCCM2 compared with controls at P6 (Fig. 5 C). These data suggest that EC proliferation is not the primary event leading to CCM malformations and does not contribute to the early vascular phenotype induced by *Ccm2* deletion.

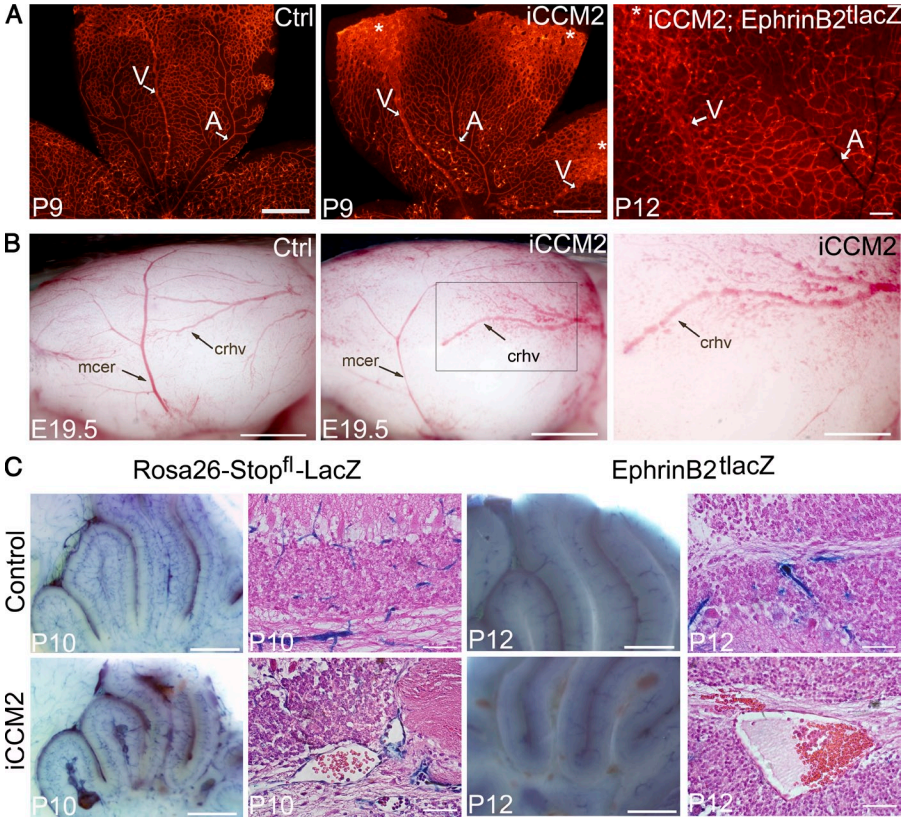

Figure 4. CCM lesions are capillary-venous and do not affect the arterial compartment. (A) Analysis at P9 or P12 of the retinal vasculature from control or iCCM2 animals using vascular isolectin-B4 staining (left and middle, n = 25 in each group analyzed between P8 and P10), after XGal staining (right, n = 4 in each group, from 2 different litters). Tamoxifen-induced *Ccm2* deletion was performed at P1. Arteries (A) are thin and normal in iCCM2 retinas, whereas veins (V) are dilated in iCCM2 animals. Asterisks show CCM lesions developing at the periphery of the retina. (B) Lateral view of cerebral hemispheres of control and iCCM2 embryos dissected at E19.5 (n = 8 in each group, from 4 different litters). *Ccm2* deletion was performed at E14.5. Vascular anomalies affect the caudal rhinal vein (crhv) and the capillaries surrounding in the iCCM2 animals. The box in the middle panel is magnified in the image on the right. (C) Analysis of the cerebellar vessels at P10 and P12 after XGal staining on whole brain (left) and after a H&E staining (right). Animals were crossed with either the *Rosa*26-Stop^{fl}-LacZ reporter mouse or the artery-specific *EphrinB2*^{tlacZ} reporter mouse. Results shown are representative of at least four animals in each group, from two different litters. Bars: 1 mm (A and B, left and middle); 500 µm (B [right] C [left]); 100 µm (A, right); 50 µm (C, right).

The pathological consequences of *Ccm2* ablation are restricted to key time points temporally related to intense angiogenesis

Ccm2 deletion at P1, a time of intense angiogenesis in the mouse retina and cerebellum (Yu et al., 1994; Plate, 1999; Acker et al., 2001; Dorrell and Friedlander, 2006) resulted in CCM lesions in both organs within a week after deletion. To assess whether the effect of *Ccm2* deletion is temporally correlated to the angiogenic process we compared deletion of *Ccm2* at P1 with deletion either at 3 wk of age, after establishment of retinal and cerebellar vessels (Acker et al., 2001; Dorrell and Friedlander, 2006), or during embryogenesis, when cerebral angiogenesis is at an intensive stage (Fig. 6; Yu et al., 1994; Plate, 1999). Tamoxifen-induced recombination efficiency was confirmed for the different protocols used (Fig. S1).

Ccm2 deletion in 3-wk-old animals did not lead to any gross cerebrovascular phenotype, as observed on iCCM2 brains upon dissection at 2 mo of age ($n = 4$; Fig. 6 A, middle). Histology performed on iCCM2 brains did not reveal any vascular lesion or any sign of hemorrhage in the cerebral hemispheres and cerebellum (unpublished data). Moreover, isolectin-B4 stainings of retinal vessels showed similar vasculature in iCCM2 and control animals (Fig. 6 B). These data show that *Ccm2* deletion at 3 wk did not lead to CCM in the mouse, suggesting that endothelial *Ccm2* is dispensable for mature vessels.

We and others have reported that endothelial-specific *Ccm2* deletion resulted in early embryonic death around embryonic day 10.5 (E10.5; Boulday et al., 2009; Whitehead et al., 2009). In the present work, tamoxifen-induced endothelial-specific *Ccm2* deletion was performed at E14.5 to bypass the early embryonic lethality. At E19.5, iCCM2 mice were distinguishable from their hemorrhagic skin (unpublished data). Upon dissection, iCCM2 brains showed vascular anomalies located on the cerebral hemispheres with irregular and tortuous rhinal cerebral veins surrounded by abnormal capillaries (Fig. 6 A, right; $n = 8$).

To get some insight into the tightness of the time-window for *Ccm2* deletion-mediated vascular effects, *Ccm2* was ablated at different postnatal time points. P4 inactivation ($n = 4$) resulted within 10 d after induction, in a milder vascular phenotype compared with P1 inactivation, which was still clearly visible upon dissection (Fig. S6 B, to be compared with Fig. S2 A). Histology of the brain showed single isolated caverns located within the cerebellum, without sign of hemorrhage (Fig. S6 E). Lesions were also observed at the periphery of the retinal vasculature (Fig. S6 H). After P8- ($n = 5$) and P15- ($n = 2$) *Ccm2* ablation, no obvious vascular phenotype was detected upon dissection in the cerebellum, at P16 and P34, respectively (Fig. 6 D and not depicted). However, histology analysis revealed vessel dilations that might precede CCM lesion development (Fig. S6 F). Isolectin-B4 stainings also showed vessel dilations at the periphery of the P8-ablated iCCM2 retinas (Fig. S6 J).

Collectively, our data on *Ccm2* deletion during embryogenesis, the postnatal period, and at 3 wk of age strongly suggested that the effects of *Ccm2* deletion on CCM lesion development were restricted to key time points temporally related to the angiogenic process.

DISCUSSION

In the present paper, we used an inducible, EC-specific deletion of the *Ccm2* gene, to bypass the embryonic lethality encountered after constitutive or endothelial-specific *Ccm2* ablation (Boulday et al., 2009; Whitehead et al., 2009).

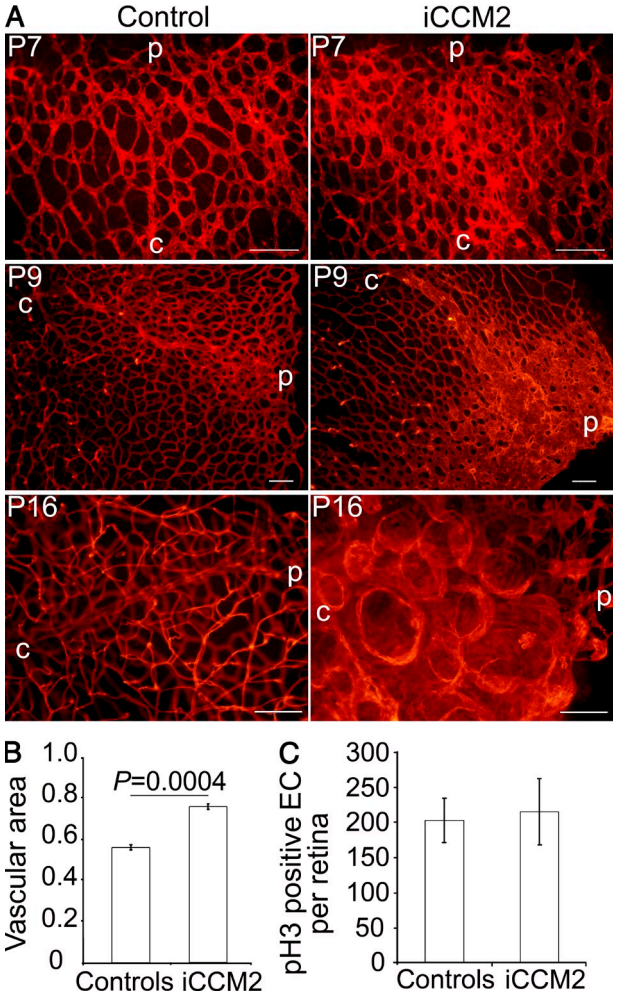

Figure 5. Natural history of the CCM lesions. (A) Retinal CCM lesion development from P7 to P16. The vasculature at the periphery of the retina on controls or iCCM2 animals is shown after isolectin-B4 staining. C, central retina; p, peripheral retina. Data are representative of at least 50 animals in each group, analyzed between P6 and P19. (B) Quantification of the vascular coverage at the venous leading edge of the plexus in the retina at P7. Data are expressed as vascular area ± SEM (isolectin-B4–positive area, relative to total retinal area analyzed; $n = 4$ in each group, from 2 different litter; 6–8 fields analyzed per retina). (C) Quantification of the EC proliferation in control or iCCM2 retinas at P6, assessed by total number of phospho-histone 3–positive ECs per retina ± SD ($n = 6$ in each group, from 3 different litters). Bars, 100 µm.

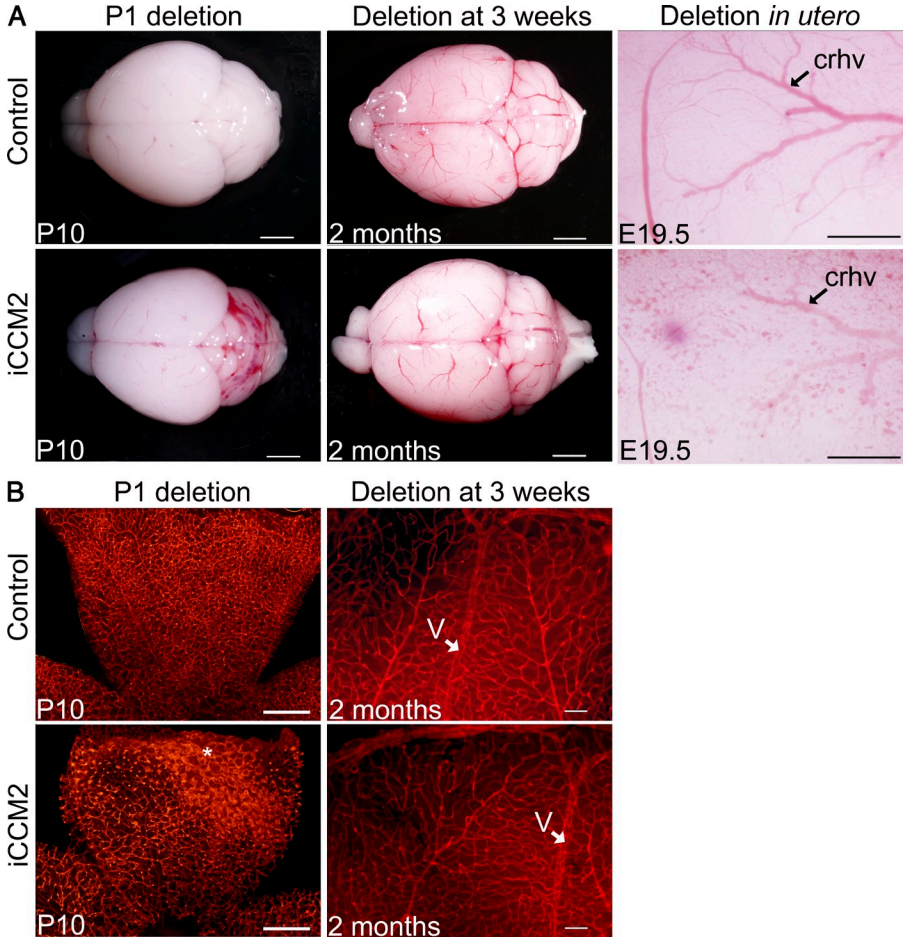

Figure 6. Timing of ablation determines endothelial response to CCM2 loss. Control and iCCM2 animals were injected with tamoxifen to delete *Ccm2* at P1 (left, $n = 25$ in each group, analyzed between P8 and P10), at 3 wk of age (middle, $n = 4$ in each group, from 3 different litters) or at E14.5 during gestation (right, $n = 8$ from 4 different litters). (A) Control and iCCM2 brains upon dissection. (B) Isolectin-B4 staining on control and iCCM2 retinas. Note the CCM lesion in the P1-induced animal (asterisks). V, vein. Bars: 2 mm (A, left and middle); 500 µm (A [right] and B [left]); 100 µm (B, right).

Early post-natal deletion of *Ccm2* resulted in vascular lesions strikingly recapitulating human CCM lesions in the brain as well as in the retina, in 100% of *Ccm2*-deleted animals. In this robust and relevant mouse model for the human CCM disease, we showed that CCM lesions affect only the venous bed and that CCM development is restricted to key time periods temporally related to intense angiogenesis.

In the past few years, different groups working in the field of CCM in vivo models concluded to a vascular, EC-specific, autonomous function of the 3 *Ccm* genes (Hogan et al., 2008; Boulday et al., 2009; Whitehead et al., 2009; He et al., 2010). Recently, a paper challenged those results showing CCM-like lesions after neuroglial-specific loss of *Ccm3*. In contrast to what was previously published, Louvi et al. (2011) demonstrated a cell autonomous effect of *Ccm3* in astrocytes, resulting in increased cell proliferation and cell survival, as well as a cell nonautonomous effect, resulting in a vascular phenotype. This data suggest that *Ccm* genes play a role in vascular and non vascular cells within the CNS, pointing out the importance of the communication between cells composing the neurovascular unit, which may partly explain the CNS restriction of the CCM lesions.

Another approach to obtain a mouse model for human CCM has been developed using genetic sensitizers, attempting to increase the rate of somatic mutation of CCM genes and obtain vascular lesions in heterozygous $Ccm1^{+/-}$ or $Ccm2^{+/-}$ mice. On a tumor repressor Trp53-null background, 30% of the $Ccm1^{+/-}$ mice developed lesions (Plummer et al., 2004), but the frequency of early onset malignancies was a limitation of this model. With a similar approach, 50% of the $Ccm1^{+/-}$ mice with a mismatch repair complex null background ($Msh2^{-/-}$; $Ccm1^{+/-}$) developed lesions (McDonald et al., 2011). No lesion was obtained in the $Msh2^{-/-}$;$Ccm2^{+/-}$ mice.

This sensitized mouse model, as well as the model from Louvi et al. (2011), has the advantage of progressing slowly, with a relative normal lifetime for the animal. In addition, according to what is thought to happen in human, lesion development in the heterozygous McDonald's model occurs as a stochastic event throughout the brain (McDonald et al., 2011). In contrast, in the model described herein, a very efficient loss of both *Ccm2* alleles is obtained in ECs, providing a more aggressive model. iCCM2 animals after P1-induction show a rapid onset of the disease, with lesion development restricted to some specific locations of the CNS, followed by an early death caused at least in part by severe hemorrhages within the CNS. However, our results using later postnatal *Ccm2* deletion (Fig. S6) suggested that a milder mouse model, useful for long term studies, could be obtained that might allow lesion development within the brain hemispheres. This will be the subject for further analysis. Finally, it would be unrealistic to expect one animal model to fully recapitulate a human phenotype and we believe that the different CCM mouse models available so far will be complementary for mechanistic exploration.

In our study, AJ and TJ organization was strongly affected in CCM2-deficient ECs in vitro and in the CCM2 lesions in vivo, consistent with the impaired TJs described in human CCM lesions. CCM2 deletion caused complex changes in AJ and TJ organization, which included down-regulation of

junctional components and alteration of their distribution at intercellular contacts. Surprisingly, endothelial cell–cell TJs were maintained in the *Msh2*$^{-/-}$; *Ccm1*$^{+/-}$ mouse model as assessed by electronic microscopy (McDonald et al., 2011). The apparent discordance between this model and our data may come from the different approaches used by the two groups. In our model, we cannot exclude that, even though we observed a down-regulation and alteration of some AJ and TJ components using immunostaining approaches, the TJ ultrastructure could be preserved. Previous studies (Whitehead et al., 2009; Stockton et al., 2010) showed that in CCM2-deficient ECs, cortical actin cytoskeleton was severely affected. This effect required the association of CCM2 with CCM1/Krit. Data presented here add to these observations and show that deletion of CCM2 causes complex changes in AJ and TJ organization, which include down-regulation of junctional components and alteration of their distribution at intercellular contacts. In a previous paper, we showed (Lampugnani et al., 2010) that similar junctions' alterations could also be observed in CCM1-depleted ECs, further supporting the idea of a physical and functional interaction between CCM1 and CCM2. One of the most striking effects of CCM2 depletion observed in our study was the strong reduction of claudin-5 expression, which is likely the cause of altered TJ organization. This effect may explain, to a good extent, the defect in permeability control of CCM2 KO ECs in vitro and in vivo (Fig. S4; Stockton et al., 2010). Furthermore, as already mentioned, TJ are severely affected in the vascular lesions of CCM patients. Genetic deletion of *claudin-5* is known to be associated to defects in blood–brain barrier (Morita et al., 1999), which leads to death immediately after birth.

Another functional consequence of alterations in AJ or TJ architecture is defective cell polarity. We previously reported that *Ccm1* silencing altered VE-cadherin and AJ organization and inhibited the localization of the polarity complex at cell–cell junctions (Lampugnani et al., 2010). As a consequence, the polarized expression of apical (podocalyxin) and basal (collagen IV) proteins was affected. In this study, although junctions are altered in vivo in CCM2 lesions, apical and basal proteins seem to be correctly distributed (Fig. S2 H). It is reasonable that because CCM1, but not CCM2, also directly interacts with integrins and modulates their functions, this additional property may be required for cell polarity (Zovein et al., 2010).

Our results clearly showed that despite pan-endothelial *Ccm2* ablation, CCM lesions did not affect all vascular beds. CCM lesions developed only in the cerebellum and the retina after P1 ablation. At the time of analysis, other highly vascularized organs, such as the heart and lungs, did not show evidence of CCM lesions upon dissection, even though Cre-mediated recombination was confirmed in those organs (unpublished data). Thus, our data clearly demonstrate that loss of *Ccm2* is not sufficient to induce CCM lesions. In addition to the complete endothelial absence of CCM2, additional factors, possibly specific for the neurovascular microenvironment, might be necessary to cause the CCM disease.

Within the brain and the retina, CCM lesions affect only the venous bed. This is consistent with what is observed in human retinal CCM lesion when using retinal angiography. The bubblelike vascular structures composing the CCM retinal lesion are the last vessels to be filled up by the fluorescent dye, suggesting that lesions are composed by pocket-like capillaries connected to the venous system. In zebrafish, *Ccm1* or *Ccm2* knockdown using morpholinos did not affect dorsal aorta and intersomitic vessel development, but resulted in abnormal morphogenesis with major dilation of the posterior cardinal vein and the caudal vein (Hogan et al., 2008). In our study, mechanisms explaining the venous restriction of CCM2 lesions remain to be elucidated. The venous-specific effect of CCM2 ablation cannot be explained by a difference in the timing of excision that would affect a vascular bed with a later development, because veins and arteries of the superficial vascular plexus develop concomitantly in the retina (Dorrell and Friedlander, 2006; Fruttiger, 2007). We then excluded a difference in recombination efficiency between veins and arteries. As assessed by XGal staining on retinas or cerebral hemispheres, P1-tamoxifen–induced recombination was clearly affecting arteries and veins to the same extent (Fig. S1, A and B). Another trivial explanation would be a venous restriction of *Ccm2* expression during late embryogenesis and the postnatal period. In a previous work, we detected a moderate labeling for all three *Ccm* transcripts in the heart, arterial, and venous large vessels by E14.5, decreasing at late embryogenic stages (Petit et al., 2006). To further address this issue, we compared CCM2 mRNA and protein expression in mesenteric arteries and veins. No significant difference in *Ccm2* gene expression level was observed in these two vascular beds at the perinatal period (unpublished data). CCM2 protein expression was also confirmed in both types of vessels (unpublished data). The venous specificity of CCM lesions could also reflect a different level of TJ component expression (i.e., claudin-5 expression) in veins versus arteries. However, claudin-5 expression, evaluated by quantitative RT-PCR was similar in mesenteric arteries and veins (unpublished data). Thus, additional work is needed to clarify what differs between veins and arteries that could explain the specific response of venous EC to *Ccm2* deletion.

The main characteristic feature of affected veins at early stages of lesion development in retinas of the iCCM2 mice was an increase in the size of the veins. To understand the mechanisms of this venous dilation, we analyzed EC proliferation before lesion formation. We did not find any enhancement in EC proliferation, suggesting that proliferation is not the primary event leading to lesions. This is consistent with what was found by other groups in the mouse as well as in the zebrafish (Hogan et al., 2008; McDonald et al., 2011). In iCCM2 cerebellum, the endothelium lining the already formed CCM lesions (single or multicavernous) did not show any increase in cell proliferation compared with endothelium from controls, as assessed by stainings for the proliferation-associated nuclear protein Ki67 at P8 and P14 (Fig. 2 J and not depicted). Our results contrast with other data, showing

an increase in proliferation of EC lining multiple mature caverns as compared with single, early cavernous lesions (McDonald et al., 2011). It is possible that the relatively short median survival in our mouse model may be a limit for analyzing EC proliferation in mature, multicavernous CCM lesions. Interestingly, loss of *Ccm1* in zebrafish resulted in impaired EC morphology rather than increase in EC proliferation, with a progressive spreading and thinning of the ECs forming the dilated vessel (Hogan et al., 2008). We do hypothesize that such a mechanism could explain the phenotype described in our CCM2 mouse model.

In this paper, we showed that the timing of *Ccm2* deletion (E14.5, P1, and 3 wk of age) defines the cerebral (or retinal) EC response to CCM2 loss. We first excluded differences in tamoxifen-induced recombination efficiency that could explain the disparate temporal and spatial responses to *Ccm2* deletion. XGal staining confirmed a high recombination efficiency at E14.5, P1, and 3 wk of age, in all the cerebral and retinal vessels (Fig. S1, A–F). Mice induced at 3 wk, after vessel development, did not develop CCM lesion in the CNS. In contrast, mice induced at P1 showed CCM lesions in the cerebellum and the retina, whereas late in utero *Ccm2* deletion elicits vascular malformations in the cerebral hemispheres. In those two situations, the location of CCM lesions in the CNS corresponds to specific places undergoing intense angiogenesis at the time of deletion (Plate, 1999; Acker et al., 2001; Dorrell and Friedlander, 2006). Thus, our results comparing the different timing of *Ccm2* deletion strongly suggest that angiogenesis might be the extra trigger leading to CCM lesion development. Interestingly, in human CCM patients, the number of lesions increases significantly with age, particularly after 50 yr old (Denier et al., 2006; Labauge et al., 2007). In addition, it has been shown that angiogenesis can occur in human adult brain in response to cerebral ischemia (Beck and Plate, 2009). We speculate that an increase in CCM lesion number over 50 yr old may be related to proangiogenic stimuli that may be caused by hypoxic events that occur with aging.

The mechanisms of this restricted temporal CCM competence are thus far unknown. In some aspects, it is reminiscent of the previously reported restricted temporal cystogenic competence of renal epithelial cells. The autosomal dominant polycystic kidney disease is characterized by a progressive increase in renal tubular diameter followed by multiple cysts formation. A key postnatal developmental switch has been involved in this cystogenic process and has been related to abnormal planar cell polarity signaling (PCP; Fischer et al., 2006; Piontek et al., 2007; Karner et al., 2009; Verdeguer et al., 2010). PCP controls, through the coupling of cell division and morphogenesis, the growth and the size of the normal renal tube. Interestingly, in the normal developing retinal vasculature, orientation of mitosis along the vessel axis was also reported (Zeng et al., 2007), suggesting that vessel growth is determined by PCP.

While this manuscript was in revision, two other studies were published (Chan et al., 2011; Cunningham et al., 2011) that independently validated the use of inducible *Ccm* KO approaches to obtain mouse models for the CCM disease. All these very recent complementary in vivo studies show similarities but also differences, most likely linked to distinct methodological approaches, which will be useful to decipher the mechanisms of CCM development.

In this study, we describe a relevant and robust mouse model for CCM disease with a complete penetrance in the CNS. We believe this model to be of importance in better deciphering molecular mechanisms involved in the CCM pathogenesis. Moreover, the rapid onset of the disease in the iCCM2 mouse model makes it particularly suitable for therapeutic preclinical evaluation, especially for a fast first screening of novel agents targeting lesion genesis. Indeed, prevention of lesion development/progression/bleeding, or induction of lesion regression are now the real challenge to pursue for the CCM disease (Yadla et al., 2010).

Herein, analysis of the iCCM2 model suggests that the loss of *Ccm2* is required and sufficient for the development of CCM lesions but only in a restricted spatial and temporal manner. We propose that, within an appropriate time window, a pro-angiogenic stimulus in the neurovascular unit microenvironment provides a permissive signal for venous EC from the CNS to eventually form CCM lesions.

MATERIALS AND METHODS

In vivo tamoxifen-induced deletion. Tamoxifen (Sigma-Aldrich) was diluted in sunflower oil-10% ethanol at 10 mg/ml, and subsequent dilutions were performed in sunflower oil when necessary. For postnatal deletion, pups were injected at P1 with a single intragastric injection of 20 µg tamoxifen. Deletion at 3 wk of age was performed by repeated i.p. injections of 1 mg tamoxifen for 4 consecutive days. For deletion during embryogenesis, pregnant females were injected once i.p. with 1 mg tamoxifen at E14.5, and a cesarean was performed at E19.5.

Mouse lines. The strategy used to target the *Ccm2* gene in mice (*Ccm2* floxed and *Ccm2* deleted alleles) was previously described (Boulday et al., 2009). *Ccm1* and *Ccm3* floxed mice were made by Taconic. The *Cdh5(PAC)*-CreERT2 mouse line was previously reported (Wang et al., 2010). The *Rosa*26-Stop^{fl}-LacZ (Soriano, 1999), *EphrinB2*^{tlacZ} (Wang et al., 1998), and BAT-Gal (Maretto et al., 2003) mice have been purchased from The Jackson Laboratory. Mice were all bred on a C57BL/6 background.

To obtain the iCCM2 mice, the *Cdh5(PAC)*-CreERT2 mice were first bred with the *Ccm2*$^{+/Del}$ animals. The *Cdh5(PAC)*-CreERT2; *Ccm2*$^{+/Del}$ mice were then crossed with *Rosa*26-Stop^{fl}-LacZ; *Ccm2*$^{fl/fl}$ animals. Thus, unless otherwise mentioned, the genotype of iCCM2 animals and controls were as follows: *Cdh5(PAC)*-CreERT2; *Ccm2*$^{fl/Del}$; *Rosa*26-Stop^{fl}-LacZ and *Cdh5(PAC)*-CreERT2; *Ccm2*$^{fl/+}$; *Rosa*26-Stop^{fl}-LacZ.

EphrinB2^{tlacZ} and BAT-Gal mice were bred with *Ccm2*$^{fl/fl}$ animals before be crossed with *Cdh5(PAC)*-CreERT2; *Ccm2*$^{+/Del}$ mice. All procedures described in this study were in full accordance with the Institutional Animal Care and Use Commitee "Lariboisiere-Villemin" (Committee number 9, Paris, France).

Cell culture. Mouse lung ECs were derived from lungs of 3-mo-old *Ccm2* $^{fl/fl}$ mice (Boulday et al., 2009) and immortalized as previously described (Dong et al., 1997; Balconi et al., 2000). Conditional deletion of *Ccm2* in vitro was obtained using TAT-Cre fusion protein which is known to promote the nuclear translocation of Cre recombinase (Peitz et al., 2002). As a control, cells were treated either with buffer or with an inactive form of TAT-Cre. Sparse ECs were washed with HyQ ADCF mAb medium (Thermo Fisher Scientific) and treated with 100 µg/ml TAT-Cre for

60 min at 37°C in HyQ ADCF mAb medium without serum, followed by 100 µM chloroquine for 60 min at 37°C (Liebner et al., 2008).

TOP/FOP assay. The assay was performed using a previously described standard technique (Taddei et al., 2008). In brief, 6×10^5 CCM2 WT and null cells were plated in 6-well plates to form 80% confluent cultures at time of transfection. Cells were transfected 24 h after seeding using the LipofectAMINE-2000 method (Invitrogen), in accordance with the manufacturer's instructions. To normalize for transfection efficiency, a pCMV-β-Gal plasmid was co-transfected. 3 µg of either TOP-TK-LUC or FOP-TK-LUC (containing WT or mutant Tcf/Lef binding sites and a basal TK promoter, upstream a luciferase gene, respectively) was used in combination with 1 µg pCMV-β-Gal. Luciferase activity was assayed 48 h after transfection, using the Enhanced Luciferase Assay kit (BD). TCF/LEF β-catenin–mediated gene transcription was defined by the ratio of TOP-TK-LUC/FOP-TK-LUC luciferase activities, where the β-Gal activity of the internal control reporter pCMV-β-Gal was used to correct differences in transfection efficiency.

Western blot analysis. Western blot analysis was performed according to standard protocols. In brief, confluent cells were washed with PBS and lysated by boiling in a modified Laemmli sample buffer (2% SDS, 20% glycerol, and 125 mM Tris-HCl, pH 6.8). Lysates were incubated for 10 min at 95°C to allow protein denaturation. The concentration of protein was determined using a BCA Protein Assay kit (Thermo Fisher Scientific) according to the manufacturer's instructions. Equal amount of proteins were loaded on gel and separated by SDS-PAGE, transferred to a Protran Nitrocellulose Hybridization Transfer Membrane 0.2 µm pore size (Whatman), and blocked for 1 h at room temperature in TBST (150 mM NaCl, 10 mM Tris-HCl, pH 7.4, and 0.05% Tween)-powdered milk. The membranes were incubated overnight at 4°C in primary antibodies diluted in TBST-5% BSA or in TBST-5% milk. Next, they were incubated for 1 h at RT with horseradish peroxidase-linked secondary antibodies (diluted in TBST-5% milk). Membranes were rinsed 3 times with TBST for 5 min each, and specific binding was detected by the enhanced chemiluminescence system (GE Healthcare) using Hyperfilm (GE Healthcare). The molecular masses of proteins were estimated relative to the electrophoretic mobility of the co-transferred, pre-stained protein marker Broad Range (Cell Signaling Technology).

Histology, β-galactosidase staining, and immunofluorescence. Brains were fixed by immersion overnight in 4% paraformaldehyde, before being paraffin-embedded. For histology analysis, hematoxylin and eosin (H&E) staining was performed on every 10 sections (10 µm each) on half-sagittal brain.

Whole-mount staining for β-galactosidase activity was performed by incubation overnight with XGal (1mg/ml solution) after 30 min fixation in cold 1% formaldehyde fixation buffer.

Immunofluorescence on frozen sections was performed after fixation in aceton or cold methanol. Sections were counterstained with DAPI and mounted in a fluorescent mounting medium (Dako). The following antibodies were used for immunohistochemistry and/or immunofluorescence: rat anti-PECAM (MEC13.3, BD); rat anti–VE-cadherin (BD); rabbit anti-ZO.1 (Zymed); rabbit anti-claudin-5 (from H. Wolburg, Institute of Pathology, University of Tubingen, Tubingen, Germany); rabbit anti-phosphohistone H3 (Abcam); peroxidase-conjugated anti–rat (Jackson ImmunoResearch Laboratories); Alexa Fluor 594–conjugated anti–rat (Invitrogen); Alexa Fluor 488–conjugated donkey anti–rabbit (Invitrogen); FITC-conjugated anti–rabbit (Jackson ImmunoResearch Laboratories).

Immunofluorescence on whole-mount retinas was performed as previously described (Pitulescu et al., 2010). Staining of retinal vessels was obtained by incubations with biotin-conjugated isolectin-B4 (AbCys) and Cy3-streptavidin (GE Healthcare). NIS-Elements imaging software (Nikon) was used to quantify vascular coverage at the venous leading edge of the retinal vasculature (vascular area relative to the total retinal area analyzed) in control and iCCM2 retinas ($n = 4$ animals with similar weight in each group, 6–8 fields per retina).

Immunofluorescence was analyzed using a Nikon Eclipse 80*i* microscope or by confocal microscopy (TCS-SP2-AOBS; Leica).

Statistics. Student's two-tailed nonpaired *t* test was used to determine statistical significance for in vitro analysis. The significance level was set at $P < 0.05$. Kaplan-Meier test was used to determine survival curve of the iCCM2 animals versus controls.

Online supplemental material. Fig. S1 shows the analysis of tamoxifen-induced recombination. Fig. S2 shows additional analysis of CCM2 lesions in the cerebellum. Fig. S3 shows the cerebellar and retinal CCM lesions obtained after *Ccm1* and *Ccm3* ablation at P1. Fig. S4 shows the analysis of AJ and TJ junctions in vitro in CCM2 KO ECs. Fig. S5 shows the analysis of molecular regulators of claudin-5 expression in vitro in CCM2 KO ECs. Fig. S6 shows the analysis of impact of the postnatal timing for *Ccm2* ablation on the vascular phenotype severity. Online supplemental material is available at http://www.jem.org/cgi/content/full/jem.20110571/DC1.

We deeply thank Eric Vicaut for the Kaplan-Meier analysis, Pierre Lacombe for FITC-Dextran perfusions, Siham Mallah and Maëlle Coquemont for excellent technical help, and Anne Joutel for very helpful discussions.

This work was supported by the Agence Nationale pour la recherche grant ANR-07-MRAR-002-01 (to E. Tournier-Lasserve), the Leducq Fondation grant 07 CVD 02 Hemorrhagic Stroke (to E. Tournier-Lasserve and E. Dejana), Institut National de la Santé et de la Recherche Médicale, and grants from the French association of CCM patients. G. Boulday is a postdoctoral fellow supported by the Leducq Foundation.

The authors have no conflicting financial interests.

Submitted: 23 March 2011
Accepted: 26 July 2011

REFERENCES

Acker, T., H. Beck, and K.H. Plate. 2001. Cell type specific expression of vascular endothelial growth factor and angiopoietin-1 and -2 suggests an important role of astrocytes in cerebellar vascularization. *Mech. Dev.* 108:45–57. doi:10.1016/S0925-4773(01)00471-3

Akers, A.L., E. Johnson, G.K. Steinberg, J.M. Zabramski, and D.A. Marchuk. 2009. Biallelic somatic and germline mutations in cerebral cavernous malformations (CCMs): evidence for a two-hit mechanism of CCM pathogenesis. *Hum. Mol. Genet.* 18:919–930.

Balconi, G., R. Spagnuolo, and E. Dejana. 2000. Development of endothelial cell lines from embryonic stem cells: A tool for studying genetically manipulated endothelial cells in vitro. *Arterioscler. Thromb. Vasc. Biol.* 20:1443–1451. doi:10.1161/01.ATV.20.6.1443

Beck, H., and K.H. Plate. 2009. Angiogenesis after cerebral ischemia. *Acta Neuropathol.* 117:481–496. doi:10.1007/s00401-009-0483-6

Bergametti, F., C. Denier, P. Labauge, M. Arnoult, S. Boetto, M. Clanet, P. Coubes, B. Echenne, R. Ibrahim, B. Irthum, et al; Société Française de Neurochirurgie. 2005. Mutations within the programmed cell death 10 gene cause cerebral cavernous malformations. *Am. J. Hum. Genet.* 76:42–51. doi:10.1086/426952

Boulday, G., A. Blécon, N. Petit, F. Chareyre, L.A. Garcia, M. Niwa-Kawakita, M. Giovannini, and E. Tournier-Lasserve. 2009. Tissue-specific conditional CCM2 knockout mice establish the essential role of endothelial CCM2 in angiogenesis: implications for human cerebral cavernous malformations. *Dis Model Mech.* 2:168–177. doi:10.1242/dmm.001263

Brunet, A., A. Bonni, M.J. Zigmond, M.Z. Lin, P. Juo, L.S. Hu, M.J. Anderson, K.C. Arden, J. Blenis, and M.E. Greenberg. 1999. Akt promotes cell survival by phosphorylating and inhibiting a Forkhead transcription factor. *Cell.* 96:857–868. doi:10.1016/S0092-8674(00)80595-4

Burgering, B.M., and G.J. Kops. 2002. Cell cycle and death control: long live Forkheads. *Trends Biochem. Sci.* 27:352–360. doi:10.1016/S0968-0004(02)02113-8

Chan, A.C., S.G. Drakos, O.E. Ruiz, A.C. Smith, C.C. Gibson, J. Ling, S.F. Passi, A.N. Stratman, A. Sacharidou, M.P. Revelo, et al. 2011. Mutations

in 2 distinct genetic pathways result in cerebral cavernous malformations in mice. *J. Clin. Invest.* 121:1871–1881. doi:10.1172/JCI44393

Clatterbuck, R.E., C.G. Eberhart, B.J. Crain, and D. Rigamonti. 2001. Ultrastructural and immunocytochemical evidence that an incompetent blood-brain barrier is related to the pathophysiology of cavernous malformations. *J. Neurol. Neurosurg. Psychiatry*. 71:188–192. doi:10.1136/jnnp.71.2.188

Craig, H.D., M. Günel, O. Cepeda, E.W. Johnson, L. Ptacek, G.K. Steinberg, C.S. Ogilvy, M.J. Berg, S.C. Crawford, R.M. Scott, et al. 1998. Multilocus linkage identifies two new loci for a mendelian form of stroke, cerebral cavernous malformation, at 7p15-13 and 3q25.2-27. *Hum. Mol. Genet.* 7:1851–1858. doi:10.1093/hmg/7.12.1851

Cunningham, K., Y. Uchida, E. O'Donnell, E. Claudio, W. Li, K. Soneji, H. Wang, Y.S. Mukouyama, and U. Siebenlist. 2011. Conditional deletion of Ccm2 causes hemorrhage in the adult brain: a mouse model of human cerebral cavernous malformations. *Hum. Mol. Genet.* 20:3198-3206.

Daly, C., V. Wong, E. Burova, Y. Wei, S. Zabski, J. Griffiths, K.M. Lai, H.C. Lin, E. Ioffe, G.D. Yancopoulos, and J.S. Rudge. 2004. Angiopoietin-1 modulates endothelial cell function and gene expression via the transcription factor FKHR (FOXO1). *Genes Dev.* 18:1060–1071. doi:10.1101/gad.1189704

Dejana, E. 2010. The role of wnt signaling in physiological and pathological angiogenesis. *Circ. Res.* 107:943–952. doi:10.1161/CIRCRESAHA.110.223750

Denier, C., S. Goutagny, P. Labauge, V. Krivosic, M. Arnoult, A. Cousin, A.L. Benabid, J. Comoy, P. Frerebeau, B. Gilbert, et al; Société Française de Neurochirurgie. 2004. Mutations within the MGC4607 gene cause cerebral cavernous malformations. *Am. J. Hum. Genet.* 74:326–337. doi:10.1086/381718

Denier, C., P. Labauge, F. Bergametti, F. Marchelli, F. Riant, M. Arnoult, J. Maciazek, E. Vicaut, L. Brunereau, and E. Tournier-Lasserve; Société Française de Neurochirurgie. 2006. Genotype-phenotype correlations in cerebral cavernous malformations patients. *Ann. Neurol.* 60:550–556. doi:10.1002/ana.20947

Dong, Q.G., S. Bernasconi, S. Lostaglio, R.W. De Calmanovici, I. Martin-Padura, F. Breviario, C. Garlanda, S. Ramponi, A. Mantovani, and A. Vecchi. 1997. A general strategy for isolation of endothelial cells from murine tissues. Characterization of two endothelial cell lines from the murine lung and subcutaneous sponge implants. *Arterioscler. Thromb. Vasc. Biol.* 17:1599–1604. doi:10.1161/01.ATV.17.8.1599

Dorrell, M.I., and M. Friedlander. 2006. Mechanisms of endothelial cell guidance and vascular patterning in the developing mouse retina. *Prog. Retin. Eye Res.* 25:277–295. doi:10.1016/j.preteyeres.2006.01.001

Faurobert, E., and C. Albiges-Rizo. 2010. Recent insights into cerebral cavernous malformations: a complex jigsaw puzzle under construction. *FEBS J.* 277:1084–1096. doi:10.1111/j.1742-4658.2009.07537.x

Fischer, E., E. Legue, A. Doyen, F. Nato, J.F. Nicolas, V. Torres, M. Yaniv, and M. Pontoglio. 2006. Defective planar cell polarity in polycystic kidney disease. *Nat. Genet.* 38:21–23. doi:10.1038/ng1701

Fontijn, R.D., O.L. Volger, J.O. Fledderus, A. Reijerkerk, H.E. de Vries, and A.J. Horrevoets. 2008. SOX-18 controls endothelial-specific claudin-5 gene expression and barrier function. *Am. J. Physiol. Heart Circ. Physiol.* 294:H891–H900. doi:10.1152/ajpheart.01248.2007

Fruttiger, M. 2007. Development of the retinal vasculature. *Angiogenesis*. 10:77–88. doi:10.1007/s10456-007-9065-1

Gault, J., R. Shenkar, P. Recksiek, and I.A. Awad. 2005. Biallelic somatic and germ line CCM1 truncating mutations in a cerebral cavernous malformation lesion. *Stroke*. 36:872–874. doi:10.1161/01.STR.0000157586.20479.fd

Glading, A.J., and M.H. Ginsberg. 2010. Rap1 and its effector KRIT1/CCM1 regulate beta-catenin signaling. *Dis. Model Mech.* 3:73–83. doi:10.1242/dmm.003293

Glading, A., J. Han, R.A. Stockton, and M.H. Ginsberg. 2007. KRIT-1/CCM1 is a Rap1 effector that regulates endothelial cell cell junctions. *J. Cell Biol.* 179:247–254. doi:10.1083/jcb.200705175

He, Y., H. Zhang, L. Yu, M. Gunel, T.J. Boggon, H. Chen, and W. Min. 2010. Stabilization of VEGFR2 signaling by cerebral cavernous malformation 3 is critical for vascular development. *Sci. Signal.* 3:ra26. doi:10.1126/scisignal.2000722

Hilder, T.L., M.H. Malone, S. Bencharit, J. Colicelli, T.A. Haystead, G.L. Johnson, and C.C. Wu. 2007. Proteomic identification of the cerebral cavernous malformation signaling complex. *J. Proteome Res.* 6:4343–4355. doi:10.1021/pr0704276

Hogan, B.M., J. Bussmann, H. Wolburg, and S. Schulte-Merker. 2008. ccm1 cell autonomously regulates endothelial cellular morphogenesis and vascular tubulogenesis in zebrafish. *Hum. Mol. Genet.* 17:2424–2432. doi:10.1093/hmg/ddn142

Karner, C.M., R. Chirumamilla, S. Aoki, P. Igarashi, J.B. Wallingford, and T.J. Carroll. 2009. Wnt9b signaling regulates planar cell polarity and kidney tubule morphogenesis. *Nat. Genet.* 41:793–799. doi:10.1038/ng.400

Labauge, P., C. Denier, F. Bergametti, and E. Tournier-Lasserve. 2007. Genetics of cavernous angiomas. *Lancet Neurol.* 6:237–244. doi:10.1016/S1474-4422(07)70053-4

Laberge-le Couteulx, S., H.H. Jung, P. Labauge, J.P. Houtteville, C. Lescoat, M. Cecillon, E. Marechal, A. Joutel, J.F. Bach, and E. Tournier-Lasserve. 1999. Truncating mutations in CCM1, encoding KRIT1, cause hereditary cavernous angiomas. *Nat. Genet.* 23:189–193. doi:10.1038/13815

Lampugnani, M.G., F. Orsenigo, N. Rudini, L. Maddaluno, G. Boulday, F. Chapon, and E. Dejana. 2010. CCM1 regulates vascular-lumen organization by inducing endothelial polarity. *J. Cell Sci.* 123:1073–1080. doi:10.1242/jcs.059329

Leblanc, G.G., E. Golanov, I.A. Awad, and W.L. Young; Biology of Vascular Malformations of the Brain NINDS Workshop Collaborators. 2009. Biology of vascular malformations of the brain. *Stroke*. 40:e694–e702. doi:10.1161/STROKEAHA.109.563692

Liebner, S., M. Corada, T. Bangsow, J. Babbage, A. Taddei, C.J. Czupalla, M. Reis, A. Felici, H. Wolburg, M. Fruttiger, et al. 2008. Wnt/beta-catenin signaling controls development of the blood-brain barrier. *J. Cell Biol.* 183:409–417. doi:10.1083/jcb.200806024

Liquori, C.L., M.J. Berg, A.M. Siegel, E. Huang, J.S. Zawistowski, T. Stoffer, D. Verlaan, F. Balogun, L. Hughes, T.P. Leedom, et al. 2003. Mutations in a gene encoding a novel protein containing a phosphotyrosine-binding domain cause type 2 cerebral cavernous malformations. *Am. J. Hum. Genet.* 73:1459–1464. doi:10.1086/380314

Louvi, A., L. Chen, A.M. Two, H. Zhang, W. Min, and M. Günel. 2011. Loss of cerebral cavernous malformation 3 (Ccm3) in neuroglia leads to CCM and vascular pathology. *Proc. Natl. Acad. Sci. USA*. 108:3737–3742. doi:10.1073/pnas.1012617108

Maretto, S., M. Cordenonsi, S. Dupont, P. Braghetta, V. Broccoli, A.B. Hassan, D. Volpin, G.M. Bressan, and S. Piccolo. 2003. Mapping Wnt/beta-catenin signaling during mouse development and in colorectal tumors. *Proc. Natl. Acad. Sci. USA*. 100:3299–3304. doi:10.1073/pnas.0434590100

McDonald, D.A., R. Shenkar, C. Shi, R.A. Stockton, A.L. Akers, M.H. Kucherlapati, R. Kucherlapati, J. Brainer, M.H. Ginsberg, I.A. Awad, and D.A. Marchuk. 2011. A novel mouse model of cerebral cavernous malformations based on the two-hit mutation hypothesis recapitulates the human disease. *Hum. Mol. Genet.* 20:211–222. doi:10.1093/hmg/ddq433

Morita, K., H. Sasaki, M. Furuse, and S. Tsukita. 1999. Endothelial claudin: claudin-5/TMVCF constitutes tight junction strands in endothelial cells. *J. Cell Biol.* 147:185–194. doi:10.1083/jcb.147.1.185

Nonaka, H., M. Akima, T. Hatori, T. Nagayama, Z. Zhang, and F. Ihara. 2002. The microvasculature of the human cerebellar meninges. *Acta Neuropathol.* 104:608–614.

Pagenstecher, A., S. Stahl, U. Sure, and U. Felbor. 2009. A two-hit mechanism causes cerebral cavernous malformations: complete inactivation of CCM1, CCM2 or CCM3 in affected endothelial cells. *Hum. Mol. Genet.* 18:911–918.

Peitz, M., K. Pfannkuche, K. Rajewsky, and F. Edenhofer. 2002. Ability of the hydrophobic FGF and basic TAT peptides to promote cellular uptake of recombinant Cre recombinase: a tool for efficient genetic engineering of mammalian genomes. *Proc. Natl. Acad. Sci. USA*. 99:4489–4494. doi:10.1073/pnas.032068699

Petit, N., A. Blécon, C. Denier, and E. Tournier-Lasserve. 2006. Patterns of expression of the three cerebral cavernous malformation (CCM) genes during embryonic and postnatal brain development. *Gene Expr. Patterns*. 6:495–503. doi:10.1016/j.modgep.2005.11.001

Piontek, K., L.F. Menezes, M.A. Garcia-Gonzalez, D.L. Huso, and G.G. Germino. 2007. A critical developmental switch defines the kinetics of kidney cyst formation after loss of Pkd1. *Nat. Med.* 13:1490–1495. doi:10.1038/nm1675

Pitulescu, M.E., I. Schmidt, R. Benedito, and R.H. Adams. 2010. Inducible gene targeting in the neonatal vasculature and analysis of retinal angiogenesis in mice. *Nat. Protoc.* 5:1518–1534. doi:10.1038/nprot.2010.113

Plate, K.H. 1999. Mechanisms of angiogenesis in the brain. *J. Neuropathol. Exp. Neurol.* 58:313–320. doi:10.1097/00005072-199904000-00001

Plummer, N.W., C.J. Gallione, S. Srinivasan, J.S. Zawistowski, D.N. Louis, and D.A. Marchuk. 2004. Loss of p53 sensitizes mice with a mutation in Ccm1 (KRIT1) to development of cerebral vascular malformations. *Am. J. Pathol.* 165:1509–1518. doi:10.1016/S0002-9440(10)63409-8

Riant, F., F. Bergametti, X. Ayrignac, G. Boulday, and E. Tournier-Lasserve. 2010. Recent insights into cerebral cavernous malformations: the molecular genetics of CCM. *FEBS J.* 277:1070–1075. doi:10.1111/j.1742-4658.2009.07535.x

Russel, D.S., and L.J. Rubinstein. 1989. Pathology of Tumors of the Nervous System. Williams & Wilkins, editor. Baltimore, MD. p. 730-736.

Soriano, P. 1999. Generalized lacZ expression with the ROSA26 Cre reporter strain. *Nat. Genet.* 21:70–71. doi:10.1038/5007

Stockton, R.A., R. Shenkar, I.A. Awad, and M.H. Ginsberg. 2010. Cerebral cavernous malformations proteins inhibit Rho kinase to stabilize vascular integrity. *J. Exp. Med.* 207:881–896. doi:10.1084/jem.20091258

Taddei, A., C. Giampietro, A. Conti, F. Orsenigo, F. Breviario, V. Pirazzoli, M. Potente, C. Daly, S. Dimmeler, and E. Dejana. 2008. Endothelial adherens junctions control tight junctions by VE-cadherin-mediated upregulation of claudin-5. *Nat. Cell Biol.* 10:923–934. doi:10.1038/ncb1752

Verdeguer, F., S. Le Corre, E. Fischer, C. Callens, S. Garbay, A. Doyen, P. Igarashi, F. Terzi, and M. Pontoglio. 2010. A mitotic transcriptional switch in polycystic kidney disease. *Nat. Med.* 16:106–110. doi:10.1038/nm.2068

Wang, H.U., Z.F. Chen, and D.J. Anderson. 1998. Molecular distinction and angiogenic interaction between embryonic arteries and veins revealed by ephrin-B2 and its receptor Eph-B4. *Cell.* 93:741–753. doi:10.1016/S0092-8674(00)81436-1

Wang, Y., M. Nakayama, M.E. Pitulescu, T.S. Schmidt, M.L. Bochenek, A. Sakakibara, S. Adams, A. Davy, U. Deutsch, U. Lüthi, et al. 2010. Ephrin-B2 controls VEGF-induced angiogenesis and lymphangiogenesis. *Nature.* 465:483–486. doi:10.1038/nature09002

Whitehead, K.J., N.W. Plummer, J.A. Adams, D.A. Marchuk, and D.Y. Li. 2004. Ccm1 is required for arterial morphogenesis: implications for the etiology of human cavernous malformations. *Development.* 131:1437–1448. doi:10.1242/dev.01036

Whitehead, K.J., A.C. Chan, S. Navankasattusas, W. Koh, N.R. London, J. Ling, A.H. Mayo, S.G. Drakos, C.A. Jones, W. Zhu, et al. 2009. The cerebral cavernous malformation signaling pathway promotes vascular integrity via Rho GTPases. *Nat. Med.* 15:177–184. doi:10.1038/nm.1911

Yadla, S., P.M. Jabbour, R. Shenkar, C. Shi, P.G. Campbell, and I.A. Awad. 2010. Cerebral cavernous malformations as a disease of vascular permeability: from bench to bedside with caution. *Neurosurg. Focus.* 29:E4. doi:10.3171/2010.5.FOCUS10121

Yu, B.P., C.C. Yu, and R.T. Robertson. 1994. Patterns of capillaries in developing cerebral and cerebellar cortices of rats. *Acta Anat. (Basel).* 149:128–133. doi:10.1159/000147567

Zawistowski, J.S., L. Stalheim, M.T. Uhlik, A.N. Abell, B.B. Ancrile, G.L. Johnson, and D.A. Marchuk. 2005. CCM1 and CCM2 protein interactions in cell signaling: implications for cerebral cavernous malformations pathogenesis. *Hum. Mol. Genet.* 14:2521–2531. doi:10.1093/hmg/ddi256

Zeng, G., S.M. Taylor, J.R. McColm, N.C. Kappas, J.B. Kearney, L.H. Williams, M.E. Hartnett, and V.L. Bautch. 2007. Orientation of endothelial cell division is regulated by VEGF signaling during blood vessel formation. *Blood.* 109:1345–1352. doi:10.1182/blood-2006-07-037952

Zhang, X., L. Gan, H. Pan, S. Guo, X. He, S.T. Olson, A. Mesecar, S. Adam, and T.G. Unterman. 2002. Phosphorylation of serine 256 suppresses transactivation by FKHR (FOXO1) by multiple mechanisms. Direct and indirect effects on nuclear/cytoplasmic shuttling and DNA binding. *J. Biol. Chem.* 277:45276–45284. doi:10.1074/jbc.M208063200

Zovein, A.C., A. Luque, K.A. Turlo, J.J. Hofmann, K.M. Yee, M.S. Becker, R. Fassler, I. Mellman, T.F. Lane, and M.L. Iruela-Arispe. 2010. Beta1 integrin establishes endothelial cell polarity and arteriolar lumen formation via a Par3-dependent mechanism. *Dev. Cell.* 18:39–51. doi:10.1016/j.devcel.2009.12.006